PHYSICAL REVIEW B **84**, 020514(R) (2011)

Enhancement of vortex pinning in superconductor/ferromagnet bilayers via angled demagnetization

Marta Z. Cieplak,[1,2] L. Y. Zhu,[2,*] Z. Adamus,[1,3] M. Kończykowski,[3] and C. L. Chien[2]
[1]*Institute of Physics, Polish Academy of Sciences, PL-02-668 Warsaw, Poland*
[2]*Department of Physics and Astronomy, The Johns Hopkins University, Baltimore, Maryland 21218, USA*
[3]*Laboratoire des Solides Irradies, École Polytechnique, F-91128 Palaiseau, France*
(Received 5 July 2011; published 29 July 2011)

We use local and global magnetometry measurements to study the influence of magnetic domain width w on the domain-induced vortex pinning in superconducting/ferromagnetic bilayers, built of a Nb film and a ferromagnetic Co/Pt multilayer with perpendicular magnetic anisotropy, with an insulating layer to eliminate the proximity effect. The quasiperiodic domain patterns with different and systematically adjustable width w, as acquired by a special demagnetization procedure, exert tunable vortex pinning on a superconducting layer. The largest enhancement of vortex pinning, by a factor of more than 10, occurs when $w \approx 0.31$ μm is close to the magnetic penetration depth.

DOI: 10.1103/PhysRevB.84.020514 PACS number(s): 74.25.Ha, 74.25.Sv, 74.78.Fk

One of the most important parameters for the application of type II superconductors is the critical current density, J_c. To achieve high J_c, it is necessary to pin vortices, which exist in the mixed state. The usual method for pinning vortices utilizes microscopic defects in the material that locally suppress superconductivity and trap normal vortex cores. Magnetic pinning (MP) instead relies on the electromagnetic interaction between the vortex magnetic field and the stray field generated by the magnetic texture in the vicinity of the superconductor surface.[1–3] Since magnetic pinning acts on a length scale comparable to the penetration depth, λ, it is dominant at temperatures close to the superconducting transition temperature, T_c, where pinning by defects becomes ineffective.

A novel magnetic pinning method utilizes a planar superconductor (S)/ferromagnet (F) bilayer (SFB) separated by a thin insulating layer, which eliminates proximity effects.[1–5] As previously suggested, the magnetic domains in the F layer create pinning centers for the vortices in the S layer so that tuning the domain structure can result in tuning J_c.[4,5] While the principle of magnetic pinning in the SFB's has been extensively discussed theoretically[2–11] and demonstrated experimentally,[12–26] the magnitude of the pinning enhancement thus far reported has been modest with a factor of no more than 3, and sometimes even suppression of pinning has been described.[18] Furthermore, it has not been feasible to compare various magnetic pinning results, since the different bilayers used in these studies would render such comparison impractical.

In this Rapid Communication, we show that it is possible to systematically vary and achieve much higher enhancement of J_c in planar SFB's with Nb as the S layer and Co/Pt multilayer with perpendicular magnetic anisotropy (PMA) as the F layer. The PMA in the F layer assures a direct effect in magnetic pinning that is not well defined in F layer with in-plane anisotropy. Using a single SFB, we use a special demagnetization method to continuously tune the width of the domains, w, in the quasiperiodic stripe domain pattern of the F layer with equal $+/-$ domain, and observe the dramatic effect of tuning on vortex pinning using the global [superconducting quantum interference device (SQUID)] and the local (Hall sensors) magnetometry measurements. Using a single SFB with an identical S layer, we have quantitatively determined J_c enhancement as a result of changing domain width. We have observed J_c enhancement in excess of 10.

The SFB's were grown by sputtering at room temperature on Si(100) substrates with the same sequence of Si(10)/Pt(10)/$[$Co(0.6)/Pt(0.3)$]_8$/Si(10)/Nb(t), with the thickness denoted in nanometers in parentheses [Fig. 1(a)]. The Si(10) layer between $[$Co/Pt$]_8$ and Nb eliminates the proximity effect. Two samples (A and B) with nominally $t = 76$ nm were studied by magnetometry, whereas the third sample (C) with $t = 20$ nm with an additional Si(10) protective layer on the top was used to extract the vortex activation energy from transport experiment, as described separately.[23] All three samples (A, B, C) display a square hysteresis loop in the normal state, with the coercive fields at 10 K of $H_c = 720$ Oe (A), 775 Oe (B), and 750 Oe (C) [Fig. 1(b)]. From magnetoresistance measurements of SFB magnetized to saturation, we extract the superconducting parameters of the Nb layer of $T_c = 8.56$ K (A), 8.42 K (B), and 7.95 K (C), coherence length, $\xi(0) =$ 14.5 nm (A), 12.4 nm (B), and 12 nm (C), and estimated Ginzburg-Landau parameter for dirty-limit superconductors[27] of $\kappa \approx 3.8$ (A), 5.2 (B), and 5.6 (C).

A well-known method for acquiring multidomains with equal $+/-$ domains in an F layer with PMA is ac demagnetization with field perpendicular to the film plane. However, we can also obtain domain pattern with equal $+/-$ domains, but with different width by demagnetization with an ac magnetic field at an angle θ with the sample plane. Figures 1(c)–1(e) show magnetic force microscopy (MFM) images of sample A at 300 K for various θ's. Indeed, the images reveal equal amount of positive and negative domains, but the average width w increases with increasing θ. From these MFM images, using two-dimensional Fourier analysis we extract the mean value of w and the standard deviation, as shown in Fig. 1(f). Demagnetization at $\theta = 0^\circ$ results in a similarly small $w \approx 0.31$–0.35 μm for all samples, but the width w increases with θ with a more rapid growth of w at small θ. This increase of w with θ is caused by the fact that in ferromagnets with PMA the magnetic moments are out-of-plane in the uniform domain area, but with an in-plane component within the domain walls.

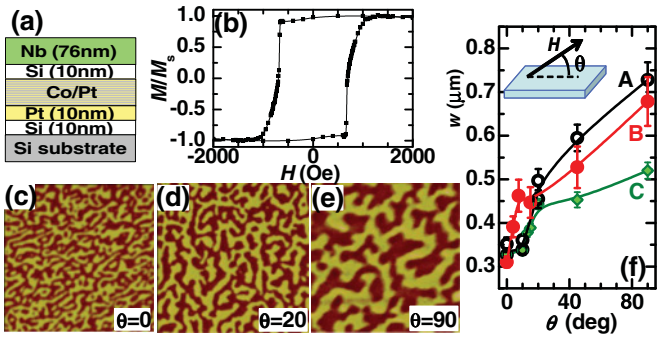

FIG. 1. (Color online) (a) Schematic of samples A and B. (b) Hysteresis loop for sample B at $T = 10$ K. (c)–(e) MFM images (10 μm $\times$ 10 μm) at 300 K for sample A demagnetized at angles $\theta = 0°$, 20°, and 90°. (f) w vs θ for samples A, B, and C (lines are guides to the eye).

With increasing θ, the demagnetization field has a decreasing in-plane component, which tends to align less spins in-plane and thus creates less domain walls, resulting in a larger w.[23] Based on the T dependence of M_s, we estimate that the domains may shrink upon cooling down to T_c by less than 10%.

As alluded to earlier, the samples A and B are nominally the same and yet they display slightly but noticeably different superconducting transition temperature T_c, coercivity H_c, coherence length $\xi(0)$, and the Ginzburg-Landau parameter κ. As shown in Fig. 1, the width w of the domains for samples A and B is also measurably different. These are unavoidable sample-to-sample variations for SFB's at these small layer thicknesses, and underscore the importance of performing the experiment with w tuning on a single SFB sample.

Figure 2(a) shows the hysteresis loops for sample B measured in a SQUID magnetometer. The loops were measured in a small external magnetic field, H, between -90 Oe and 90 Oe, after setting the domain pattern by ac demagnetization at angle θ followed by cooling the sample just below T_c. The cycling of the small magnetic field has no effect on the domain pattern, and no relaxation of magnetization in the superconducting state has been observed. Also included in Fig. 2(a), with the narrowest hysteresis loop, is the sample with a saturated F layer. The width of the hysteresis loop, ΔM, increases dramatically as a result of demagnetization, indicating a large enhancement of vortex pinning by the magnetic domains. The largest ΔM is at $\theta = 0°$, when w is small, and decreases as w grows with increasing θ. Even at $\theta = 90°$ with the largest w of about 0.7 μm, ΔM is still much larger than that of the saturated F layer. We have also observed a slight asymmetry in the hysteresis curve, particularly at large θ.

To estimate the enhancement of J_c from the global magnetometry results, one needs a model of the critical state with a specific dependence of J_c on the magnetic induction B. The simplest is the Bean model, which assumes J_c to be independent of B, leading to the well-known prediction of $J_c \sim \Delta M$.[28] Under this model, the ratio $\Delta M_\theta / \Delta M_{\rm sat} \equiv G$ reflects the enhancement of J_c induced by the domain pattern as set by the demagnetization, where ΔM_θ and $\Delta M_{\rm sat}$ are the hysteresis loop width for a sample demagnetized at θ and that of the saturated F layer, respectively. The dependence of

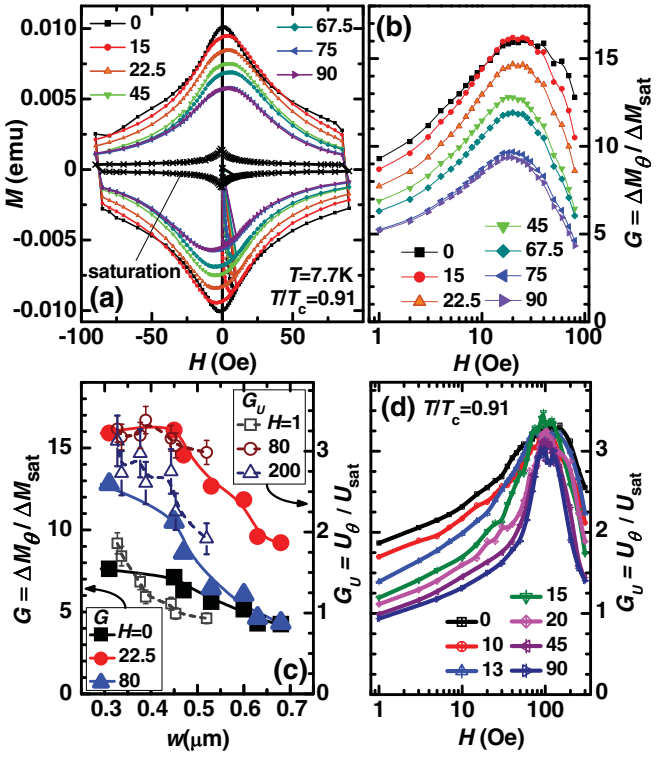

FIG. 2. (Color online) (a) Hysteresis loops measured with a SQUID magnetometer after demagnetization of sample B with $\theta = 0°$, 15°, 22.5°, 45°, 67.5°, 75°, and 90° and after saturation (from the outermost to the innermost loop, respectively). Note that loops for 75° and 90° almost overlap. (b) $G = \Delta M_\theta / \Delta M_{\rm sat}$ vs H for $\theta = 0°$, 15°, 22.5°, 45°, 67.5°, 75°, and 90° (from top to bottom). (c) $G = \Delta M_\theta / \Delta M_{\rm sat}$ (left scale) vs w for $H = 0$ (full squares), $H = 22.5$ Oe (full circles), and $H = 80$ Oe (full triangles); and $G_U = U_\theta / U_{\rm sat}$ for sample C, from Ref. 23, (right scale) vs w for $H = 1$ Oe (open squares), $H = 80$ Oe (open circles), and $H = 200$ Oe (open triangles). (d) $G_U = U_\theta / U_{\rm sat}$ vs H, extracted from the transport experiment for sample C,[23] for $\theta = 0°$, 10°, 13°, 15°, 20°, 45°, and 90° (from top to bottom).

G on H is shown in Fig. 2(b) on a semilogarithmic scale, omitting the same dependence for negative H. The $G(H)$ dependencies are similar for various θ. The largest value of $G \approx 16$ is observed for small θ in the intermediate field range of $H \sim 15$–30 Oe. The value of G at all fields decreases with increasing of θ, but still retains a high peak value of $G \approx 9$ at $\theta \approx 90°$. Figure 2(c) shows the dependence of G (left scale, full data points) on the actual domain width w for three representative field values, at the peak ($H = 22.5$ Oe), low H ($H = 0$), and high H ($H = 80$ Oe). The G is reduced almost linearly with increasing w at low H (bottom curve). At the peak (top curve), the G remains large for narrow domains, and starts to decrease rapidly for w exceeding about 0.45 μm. The high-H behavior (middle curve) is intermediate, with the weak suppression of G for small w, and more rapid suppression for large w.

To obtain a model-independent assessment of J_c, we need microscopic measurement of B at various locations. For this purpose, we employ a linear array of miniature Hall sensors to probe locally the dependence of B on the distance x from the sample edge. The local magnetic field is defined as

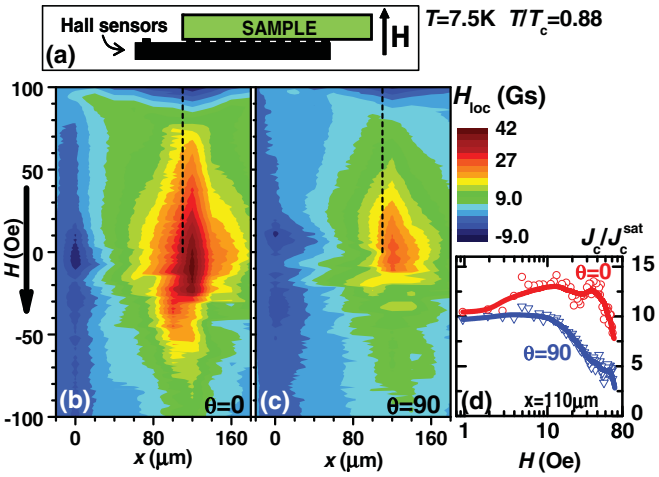

FIG. 3. (Color online) (a) Placement of the sample, with Nb adjacent to Hall sensors. (b),(c) $H_{\rm loc}(x,H)$ for sample A during the field sweep from +100 Oe to −100 Oe for $\theta = 0^\circ$ and $\theta = 90^\circ$. The edge and the center of the sample strip are at $x = 0$ and 120 μm, respectively. (d) $J_c/J_c^{\rm sat}$ vs H calculated for $x = 110$ μm [x shown by dashed line in (b) and (c)].

$H_{\rm loc} = B - \mu_0 H$, and J_c is obtained from the relation $\mu_0 J_c \approx 2dB/dx$.[29] From sample A, we cut a 240-μm-wide strip and placed a line of 10 sensors, each of which was 5×5 μm^2 in size and 20 μm apart, across the strip. An additional sensor, placed a few mm outside the sample edge, is used to measure the actual applied field as shown in Fig. 3(a). The $B(x)$ is registered simultaneously by Hall sensors, while H is swept from 0 up to +100 Oe, and from +100 Oe to −100 Oe. The evolution of $H_{\rm loc}(x)$ during the second part of the sweep is shown in Figs. 3(b) and 3(c) for $\theta = 0^\circ$ and 90°. As H is swept, the flux remains trapped inside, so that $H_{\rm loc}$ increases in the sample center, eventually reaching a maximum of 41 Oe ($\theta = 0^\circ$) or 27 Oe ($\theta = 90^\circ$) just after H changes sign to negative, while in the saturated sample 5.5 Oe is observed. The calculated J_c has a maximum at approximately the same H, reaching about 1.5×10^8 A m^{-2} for $\theta = 0^\circ$, and 8.4×10^7 A m^{-2} for $\theta = 90^\circ$, while it is only 1.6×10^7 A m^{-2} in the saturated sample. This confirms the conclusion of strong pinning enhancement, particularly for narrow domains at $\theta = 0^\circ$. Interestingly, Figs. 3(b) and 3(c) reveal that the change of $H_{\rm loc}$ is much smoother during the sweep from +100 Oe to 0 than during the sweep from 0 to −100 Oe, where there are many sudden and large drops of $H_{\rm loc}$ across the whole sample. Such an abrupt decrease of $H_{\rm loc}$ indicates the abrupt annihilation of flux over the large sample area. It is most likely triggered by the strong interaction between the positive flux still trapped inside and negative flux entering the sample. This effect likely contributes to the asymmetry of hysteresis seen in Fig. 2(a).

Figure 3(d) shows the ratio of J_c to $J_c^{\rm sat}$ (where $J_c^{\rm sat}$ is J_c in the saturated sample), calculated for $x = 110$ μm, the approximate position at which dB/dx is the largest [along the dashed line in Figs. 3(b) and 3(c)]. The calculation has been made for $H > 0$, since, for negative H, J_c is highly irregular because of the jumps of $H_{\rm loc}$. As shown in Fig. 3(d), $J_c/J_c^{\rm sat}$ is higher for $\theta = 0^\circ$ in the whole H range than that for $\theta = 90^\circ$, the same conclusion as that in Fig. 2(b), although the shape of $J_c/J_c^{\rm sat}$, while generally similar to $G(H)$ in Fig. 2(b), differs noticeably in details. This is not surprising because the local measurements using an array of Hall sensors are more susceptible to local irregularities of the flux penetration inside the narrow sample, while the global magnetometry measurement integrates over the large sample. Nevertheless, the most essential conclusion that pinning is strongest for narrow domains remains unchanged. A similar result is obtained at lower T, but the maximal magnitude of the $J_c/J_c^{\rm sat}$ decreases, by about 17% at $T/T_c = 0.82$ and by 30% at $T/T_c = 0.78$.

The results clearly establish that the strongest pinning occurs at the smallest w. This is due to several factors. The magnitude of the stray field at the domain center scales as $1/w$,[30] and, moreover, the density of pinning centers also increases with decreasing w. As a result, at low H the vortices are most effectively pinned when w is the smallest. An additional argument comes from the comparison of w to the penetration depth, since this is the length scale of the vortex-domain interaction. The thickness of Nb in sample B is $t = 76$ nm, slightly larger than $\lambda(0) \approx \kappa\xi(0) \approx 64$ nm. As T increases, $\lambda(T)$ grows as $\sim \kappa\xi(0)/\sqrt{1 - T/T_c}$, so at $T/T_c = 0.91$, we obtain $\lambda \approx 220$ nm. However, at high T, one approaches the limit of $\lambda \gg t$, for which one should use the effective penetration depth, $\Lambda = \lambda^2/t \approx 640$ nm.[27] While this higher limit is not quite reached here, it is likely that λ approaches, and perhaps even exceeds, the average domain width of $w \approx 310$ nm for $\theta = 0^\circ$. Since in the quasiordered domain pattern there are areas in which w is smaller than average, vortices cannot move freely along domains, thus enhancing the pinning. The value of w grows with increasing θ and the vortices flow more easily, thus diminishing the value of G.

As shown in Fig. 2(b), for each value of θ, G increases with H, reaching a maximum presumably when the vortex lattice becomes commensurate with the magnetic domain pattern. This is followed by a decrease of G, when the vortex density exceeds that of the domain-induced pinning centers. Since the domain density decreases with increasing w, the suppression of G at high H is weaker for smaller w as shown by the blue triangles in Fig. 2(c).

The commensurability of vortex pinning can be advantageously observed using an ordered array of pinning centers, which lead to enhanced pinning at well-defined matching fields.[1] In the SFBs, the vortices are confined to the irregular domains of one sign. In the case of a regular stripe domain pattern with the period $2w$, single or multiple chains of vortices are pinned by each domain, as recently shown by scanning tunneling microscopy.[22] We have recently performed transport measurements on sample C demagnetized at different θ to capture different domain widths and we have inferred a similar chain-pinning phenomenon.[23] At T sufficiently below T_c, the resistance is thermally activated, with the activation energy for vortex pinning, U, enhanced by magnetic domains. The $U(H)$ exhibits maxima at matching fields when narrow domains (small θ) pin single vortex chains and wider domains (large θ) pin double vortex chains.

It is interesting to compare the activation energy U from transport measurements on sample C[23] with the present data on sample B. From the transport results, we calculate the

enhancement of U induced by demagnetization at $T/T_c = 0.91$, using the parameter $G_U = U_\theta / U_{\rm sat}$, where U_θ is for sample C demagnetized at θ and $U_{\rm sat}$ is for the saturated sample. The values of G_U versus H for several values of θ are shown in Fig. 2(d). One notes that G_U and G display strikingly similar H dependence. Furthermore, both display the largest value at the smallest values of θ, decreasing monotonically with increasing θ. These systematic dependencies are illustrated in Fig. 2(c), where G (filled symbols) and G_U (open symbols) are for three representative fields, from the low field, peak, and high field regions ($H = 0$, 22.5, and 80 Oe for G, and $H = 1$, 80, and 200 Oe for G_U, respectively). The qualitative similarity suggests a common origin, which is pinning of vortex chains by domains.

However, there are also noticeable differences between $G(H)$ and $G_U(H)$. One notes that the peak in $G_U(H)$ has a narrower width but it is located at a higher H than that of $G(H)$, whereas G reaches a maximum magnitude about five times larger than that of G_U. Most of these differences are due to the different Nb thickness in sample B (76 nm) for $G(H)$ and sample C (20 nm) for $G_U(H)$. In addition, sample B shows larger dispersion of w. The dispersion of w contributes directly to the broadening of the matching field, while a thicker Nb layer leads to a progressive reduction of the domain-induced stray field (by up to about 25% on the other side of Nb[30]), and therefore reduction of the density of pinning centers across t, shifting the $G(H)$ peak to smaller H. The difference in magnitude between G and G_U is also mainly related to thickness. The strength of the magnetic interaction roughly depends on the ratio of the domain width w to the range of magnetic interaction, given approximately by Λ. In the thicker sample B, the magnetic interaction is stronger because w is comparable to Λ, whereas in the thinner sample C, Λ is about four times larger, so that the magnetic interaction is substantially reduced.

In conclusion, we have demonstrated a method to induce large enhancement of vortex pinning in the superconductor/ferromagnet bilayers using a ferromagnetic layer with perpendicular magnetic anisotropy. By demagnetizing the sample at an angle to the sample surface, we obtain domain patterns with equal $+/-$ domains but different domain width w. This unique attribute allows a single bilayer to acquire different domain widths to exert tunable vortex pinning on a superconducting layer. Magnetometry and local measurements using an array of Hall sensors show conclusively vortex pinning enhancement, by a factor of more than 10 at domain width w of about 310 nm, much larger than previously obtained.

This work was supported by Polish MNiSW Grant No. N202 058 32/1202, by NSF Grant No. DMR05-20491, by the French-Polish Bilateral Program PICS 4916, and by the European Union within the European Regional Development Fund, through the Innovative Economy Grant No. POIG.01.01.02-00-108/09.

*Current address: Materials Science Division, Argonne National Laboratory, Argonne, IL 60439.

[1] M. Velez, J. I. Martín, J. E. Villegas, A. Hoffmann, E. M. González, J. L. Vicent, and Ivan K. Schuller, J. Magn. Magn. Mater. **320**, 2547 (2008).

[2] I. F. Lyuksyutov and V. L. Pokrovsky, Adv. Phys. **54**, 67 (2005).

[3] A. Yu. Aladyshkin, A. V. Silhanek, W. Gillijns, and V. V. Moshchalkov, Supercond. Sci. Technol. **22**, 053001 (2009).

[4] L. N. Bulaevskii, E. M. Chudnovsky, and M. P. Maley, Appl. Phys. Lett. **76**, 2594 (2000).

[5] Yu. I. Bezpyatykh, W. Wasilevski, M. Gajdek, I. P. Nikitin, and S. A. Nikitov, Sov. Phys. Solid State **43**, 1827 (2001).

[6] M. V. Milosevic, S. V. Yampolskii, and F. M. Peeters, Phys. Rev. B **66**, 174519 (2002).

[7] S. Erdin, I. F. Lyuksyutov, V. L. Pokrovsky, and V. M. Vinokur, Phys. Rev. Lett. **88**, 017001 (2002).

[8] E. B. Sonin, Phys. Rev. B **66**, 136501 (2002).

[9] R. Laiho, E. Lahderanta, E. B. Sonin, and K. B. Traito, Phys. Rev. B **67**, 144522 (2003).

[10] M. A. Kayali and V. L. Pokrovsky, Phys. Rev. B **69**, 132501 (2004).

[11] S. Erdin, Phys. Rev. B **73**, 224506 (2006).

[12] A. Garcia-Santiago, F. Sanchez, M. Varela, and J. Tejada, Appl. Phys. Lett. **77**, 2900 (2000).

[13] X. X. Zhang, G. H. Wen, R. K. Zheng, G. C. Xiong, and G. J. Lian, Europhys. Lett. **56**, 119 (2001).

[14] D. B. Jan, J. Y. Coulter, M. E. Hawley, L. N. Bulaevskii, M. P. Maley, Q. X. Jia, B. B. Maranville, F. Hellman, and X. Q. Pan, Appl. Phys. Lett. **82**, 778 (2003).

[15] M. Lange, M. J. Van Bael, V. V. Moshchalkov, and Y. Bruynseraede, Appl. Phys. Lett. **81**, 322 (2002).

[16] M. Z. Cieplak, X. M. Cheng, C. L. Chien, and Hai Sang, J. Appl. Phys. **97**, 026105 (2005).

[17] M. Z. Cieplak, Z. Adamus, A. Abal'oshev, I. Abal'osheva, M. Berkowski, X. M. Cheng, Hai Sang, and C. L. Chien, Phys. Status Solidi C **2**, 1650 (2005).

[18] M. Feigenson, L. Klein, M. Karpovski, J. W. Reiner, and M. R. Beasley, J. Appl. Phys. **97**, 10J120 (2005).

[19] V. Vlasko-Vlasov, U. Welp, G. Karapetrov, V. Novosad, D. Rosenmann, M. Iavarone, A. Belkin, and W.-K. Kwok, Phys. Rev. B **77**, 134518 (2008).

[20] A. Belkin, V. Novosad, M. Iavarone, J. Pearson, and G. Karapetrov, Phys. Rev. B **77**, 180506 (2008).

[21] V. K. Vlasko-Vlasov, U. Welp, A. Imre, D. Rosenmann, J. Pearson, and W. K. Kwok, Phys. Rev. B **78**, 214511 (2008).

[22] G. Karapetrov, M. V. Milošević, M. Iavarone, J. Fedor, A. Belkin, V. Novosad, and F. M. Peeters, Phys. Rev. B **80**, 180506(R) (2009).

[23] L. Y. Zhu, M. Z. Cieplak, and C. L. Chien, Phys. Rev. B **82**, 060503(R) (2010).

[24] V. Vlasko-Vlasov, U. Welp, W. Kwok, D. Rosenmann, H. Claus, A. A. Buzdin, and A. Melnikov, Phys. Rev. B **82**, 100502(R) (2010).

[25] M. Iavarone, A. Scarfato, F. Bobba, M. Longobardi, G. Karapetrov, V. Novosad, V. Yefremenko, F. Giubileo, and A. M. Cucolo, Phys. Rev. B **84**, 024506 (2011).

[26]C. Visani, P. J. Metaxas, A. Collaudin, B. Calvet, R. Bernard, J. Briatico, C. Deranlot, K. Bouzehouane, and J. E. Villegas, e-print arXiv:1107.1122v1.

[27]M. Tinkham, *Introduction to Superconductivity* (Dover, New York, 2004).

[28]C. P. Bean, Phys. Rev. Lett. **8**, 250 (1962); Rev. Mod. Phys. **36**, 31 (1964).

[29]E. H. Brandt, Phys. Rev. B **54**, 4246 (1996).

[30]G. M. Maksimova, R. M. Ainbinder, and D. Y. Vodolazov, Phys. Rev. B **78**, 224505 (2008).